Palaeogeography, Palaeoclimatology, Palaeoecology 306 (2011) 41–57

Contents lists available at ScienceDirect

Palaeogeography, Palaeoclimatology, Palaeoecology

journal homepage: www.elsevier.com/locate/palaeo

The Valanginian isotope event: A complex suite of palaeoenvironmental perturbations

Benjamin Gréselle [a,*], Bernard Pittet [a], Emanuela Mattioli [a], Michael Joachimski [b], Nicolas Barbarin [c], Laurent Riquier [d], Stéphane Reboulet [a], Emmanuelle Pucéat [d]

[a] UMR CNRS 5276 LGL-TPE, Université Claude Bernard Lyon 1, Ecole Normale Supérieure Lyon, 69622 Villeurbanne cedex, France
[b] Institut für Geologie une Mineralogie, Universität Erlangen, Schlossgarten 5, 91054 Erlangen, Germany
[c] CEREGE, UMR CNRS 6635, Université Aix-Marseille, BP 80, 13545 Aix-en-Provence cedex 04, France
[d] UMR CNRS 5561 Biogéosciences, Université de Bourgogne, 6 Boulevard Gabriel, 21000 Dijon, France

ARTICLE INFO

Article history:
Received 21 July 2010
Received in revised form 21 March 2011
Accepted 21 March 2011
Available online 26 March 2011

Keywords:
Carbonate production crisis
$\delta^{13}C$ Weissert Event
Accumulation rates
Climate change
Valanginian

ABSTRACT

The Valanginian records a severe crisis of carbonate systems, both on platforms and in the pelagic realm. This crisis is roughly concomitant with the Weissert Event, characterized by a positive $\delta^{13}C$ excursion of about 2‰ in marine carbonates. However, it is unclear if the response of these two carbonate systems to the global perturbations is contemporaneous, or if they react differently. For this purpose, accumulation rates of pelagic carbonates produced by nannofossils and of platform-derived carbonates have been quantified in a hemipelagic environment (the Vocontian Basin, SE France) that has the potential to record the reaction of both shallow-water and pelagic carbonate production to a major perturbation of the carbon cycle, testified by the isotope excursion. Also, changes through time of clay input have been measured in order to evaluate variations in continental weathering rates, and thus in continent-derived nutrient input and climatic conditions in terms of humidity/aridity. Accumulation rates of pelagic carbonates, of platform-derived carbonates and of clays were calculated on the basis of nannofossil absolute abundance and species-specific masses, of weight percent carbonate content of rocks, and a high-resolution timescale given by cyclostratigraphy. The onset of the positive $\delta^{13}C$ excursion and the demise of the platforms testify for a synchronous, but inverse response of the shallow-water and pelagic carbonate systems to an increase in nutrient influx to marine waters. As carbonate production by nannofossils decreased during the Late Valanginian in time of still low platform production, the low temperature of marine waters coeval to a still high nutrient input recorded in the latest Late Valanginian possibly could explain that both platform and pelagic carbonate production contemporaneously decreased.

1. Introduction

The Valanginian records an important perturbation of the carbon cycle, as indicated by a positive excursion of $\delta^{13}C_{carb}$ known as the 'Weissert Event' (Erba et al., 2004). This event was recorded worldwide, in the Atlantic (Cotillon and Rio, 1984; Wortmann and Weissert, 2000; Adatte et al., 2001) and Pacific (Bartolini, 2003; Erba et al., 2004) Oceans, as well as in Northwest Siberia (Price and Mutterlose, 2004). In the Tethyan Realm, the Weissert Event was documented in northern Italy (Lini et al., 1992; Channell et al., 1993; Lini, 1994; Sprovieri et al., 2006), in the Helvetic domain (Föllmi et al., 1994), and in the Vocontian Basin (Hennig et al., 1999; van de Schootbrugge et al., 2000; Duchamp-Alphonse et al., 2007; McArthur et al., 2007). Besides these numerous marine records, the positive isotope excursion was also documented in continental flora of southern Crimea; thus both ocean and atmosphere reservoirs were affected by the perturbation in the carbon cycle (Gröcke et al., 2005). The Weissert Event is concomitant with a significant cooling indicated by glendonite record (Price, 1999), oxygen isotopes of fish teeth enamel (Pucéat et al., 2003), and Mg/Ca ratios of the belemnite calcite (McArthur et al., 2007). Simultaneously, an increase in phosphorus accumulation rate occurred in the Helvetic and Vocontian realms (Föllmi, 1995; van de Schootbrugge et al., 2003), and rare and thin organic-rich layers were deposited in the Tethys, Atlantic and Pacific Oceans (Summerhayes and Masran, 1983; Stein et al., 1986; Bersezio et al., 2002; Bralower et al., 2002; Reboulet et al., 2003) although ocean-wide dysaerobic conditions seem unlikely for this period (Westermann et al., 2010).

Carbonate platforms were also profoundly affected by the Valanginian palaeoenvironmental perturbations, and commonly exhibit a change from coralgal to bryomol facies (Funk et al., 1993; Föllmi, 1996; Föllmi et al., 2006; Gréselle and Pittet, 2010). This change in carbonate producers generally preceded the total demise of carbonate platforms of both the Tethys and the North Atlantic Oceans, as documented by Masse and Philip (1981), Schlager (1981), Harris et al. (1984), Föllmi et al. (1994), and Weissert et al. (1998). This carbonate production crisis on platforms seems to correspond to a biocalcification decrease in basinal

* Corresponding author.
E-mail address: benjamin.greselle.pro@gmail.com (B. Gréselle).

0031-0182/$ – see front matter © 2011 Elsevier B.V. All rights reserved.
doi:10.1016/j.palaeo.2011.03.027

settings, as suggested by the Nannoconid decline, i.e. a drop in the abundance of the rock-forming calcareous nannofossil *Nannoconus* (Erba and Tremolada, 2004). However, it is uncertain if the biocalcification crisis started at the same time in the pelagic realm and on platforms, affecting the whole-ocean carbonate reservoir simultaneously.

Because of their proximity to shallow-water domains, epicontinental basins provide the unique opportunity to test the synchronicity of fluctuations in both platform and pelagic carbonate production. As Valanginian calcareous nannofossils were the main carbonate producers in the ocean realm, accumulation rate of pelagic carbonates (μm yr^{-1}) are quantified by combining (1) an estimation of nannofossil abundance per gram of rock, with (2) the specific volume of the most abundant and biggest taxa, (3) the total accumulation rate of sediments, and (4) the total carbonate content of the analyzed samples. Knowing the fraction of carbonate produced by nannofossils, the accumulation rate of non-pelagic carbonates, likely derived from adjacent platforms and exported basinwards, is calculated. Clay accumulation rate can be thus appraised, and changes in siliciclastic input through time provides information on the intensity of continental weathering and runoff and, ultimately, on climate conditions prevailing in the studied region.

The Vocontian Basin (SE France) is here selected because of its small size (about 150 km in width; Cotillon et al. (1980)) and its bathymetry (a few hundred meters; Wilpshaar et al. (1997)), important enough for a development of calcareous nannoplankton community comparable with open-ocean sites. The basin was surrounded by carbonate platforms where carbonate mud was produced and exported offshore (Reboulet et al., 2003; Gréselle and Pittet, 2010). The present work aims to quantify accumulation rates of pelagic carbonates, of platform-derived carbonates, and of clays in order (1) to compare the reaction of both platform and pelagic carbonate systems in times of a global carbon cycle perturbation; (2) to precisely assess the tempo and modes in the response of both platform and pelagic carbonate production to this perturbation.

2. Geological framework and cyclostratigraphy

The analyzed sections of Vergol, La Charce and Morenas are located in the central part of the Vocontian Basin (Fig. 1b), and are well-dated by ammonite and nannofossil biostratigraphy (Reboulet et al., 1992; Reboulet, 1996; Reboulet and Atrops, 1999; Reboulet et al., 2003). In order to obtain a complete cyclostratigraphic framework and avoid local sedimentary perturbations (slumps) the three sections (Fig. 1b) were combined into a composite section. These sections can be correlated with each other bed-by-bed, and also with the well-studied, parastratotype at Angles (Fig. 1b) located some 100 km to the South of the analyzed sections (Figs. 1c and 2). The long-distance correlation of the marl–limestone alternations in the Vocontian Basin shows that they have a primary origin, and demonstrates that they cannot result from a diagenetic redistribution of carbonates, as previously proposed for the Faisceau médian by Munnecke et al. (2001).

Time estimates used in this study follows the cyclostratigraphic framework of Gréselle and Pittet (2010) that slightly differs from that of Giraud et al. (1995) who did not identify a hierarchy of cycles in the Angles section. Gréselle and Pittet (2010) recognized a hierarchy between three orders of depositional cycles allowing them to propose an orbital control for the formation of lithological cycles. These cycles can be defined as depositional sequences sensu Strasser et al. (1999) in comparison with shallow-water environments. Elementary sequences correspond to 20 ka precession cycles, small-scale sequences to 100 ka short-term eccentricity cycles, and medium-scale to 400 ka long-term eccentricity cycles (Gréselle and Pittet, 2010). This interpretation suggests a duration of 4.7 Myr for the Valanginian. This estimate is fairly consistent with the recent geochronological timescales of Gradstein et al. (1994, 2004) although it differs significantly from the 6.3 Myr inferred by Ogg et al. (2008).

3. Materials and methods

3.1. Nannofossil absolute abundance and assemblage composition

A total of 174 samples have been analyzed for this study. Sample spacing was very close (every 5 cm) in some marl–limestone alternations or intervals characterized by lithological changes (Fig. 3). Samples were taken at a lower rate for the rest of the section with at least two samples studied for each marl–limestone alternation. Samples were treated for total wt.% $CaCO_3$ content and for nannofossil absolute abundance. Smear slides for nannofossil analyses were prepared following the random settling technique described by Beaufort (1991), Geisen et al. (1999) and slightly modified by Olivier et al. (2004), in order to calculate the number of nannofossils (coccoliths and nannoliths) per gram of rock.

On average, 320 nannofossils per sample (minimum 200 specimens in a few, poor samples, and a maximum of 516 specimens in the richest one), both coccoliths and nannoliths, were counted under a polarizing-light microscope (1250×) over a variable surface area (1×10^{-3} to 256×10^{-3} cm^2) according to the richness of nannofossils in the slide. In one single sample, only 123 specimens could be counted, due to the paucity of nannofossils. A total of 110 different taxa were determined taxonomically. When applying a simple rarefaction graph to the counted specimens (x axis) with respect to the species richness (y axis) recorded in each sample, 320 specimens are largely sufficient to stabilize the number of the achieved species in a sample. The relative abundance of *Nannoconus* (percentage) is also calculated in different samples. Three preservation classes (relatively poor, moderate and good) were recognized on the basis of etching and overgrowth of the specimens, as established by Roth (1984).

3.2. Nannofossil flux and accumulation rates of pelagic and non-pelagic carbonates, and of clays

Total nannofossil flux, as well as coccolith and nannolith fluxes have been estimated by combining total accumulation rate and nannofossil abundance per gram of rock, and are expressed as number of specimens per square meter. Total accumulation rate (both carbonates and clays) was calculated using the thickness of the marl–limestone alternations and their duration as they formed in tune with precession cycle (average duration of 20 kyr in the Early Cretaceous; Berger and Loutre, 1994). Carbonate content (% weight of bulk rock) was analyzed using a Dietrich-Frühling calcimeter to determine $CaCO_3$ contents by measuring evolved CO_2 after acidification of the samples. This carbonate content combined to total accumulation rate allowed calculation of both carbonate and clay accumulation rates. By combining the relative abundance of the different nannofossil species and their specific masses (Table 1) with the total abundance of nannofossils per gram of rock, the pelagic carbonate fraction produced by nannofossils was calculated per gram of sediment. Knowing the accumulation rate of the carbonates (both pelagic and non-pelagic) and the pelagic carbonate fraction, the accumulation rates of non-pelagic carbonates was also calculated (expressed in μm yr^{-1}).

Masses of the most abundant Early Cretaceous nannofossil taxa have been estimated by Tremolada and Young (2002) and Bornemann et al. (2003) using biometric analysis, and the masses of a few other species are provided in Erba and Tremolada (2004) (Table 1). For a same species, the masses obtained by Tremolada and Young (2002) are generally greater than those determined by Bornemann et al. (2003) except for *Watznaueria barnesiae*, one of the most common taxa of the Early Cretaceous (Williams and Brawlower, 1995; Erba and Tremolada, 2004; Lees et al., 2005; Mutterlose et al., 2005). Both masses have been tested in the present work. When the largest masses of taxa were applied, the pelagic carbonate fraction often exceeded 100% of total carbonate. Therefore, the smallest mass for each taxon was applied for the calculations. Furthermore, the biggest taxon

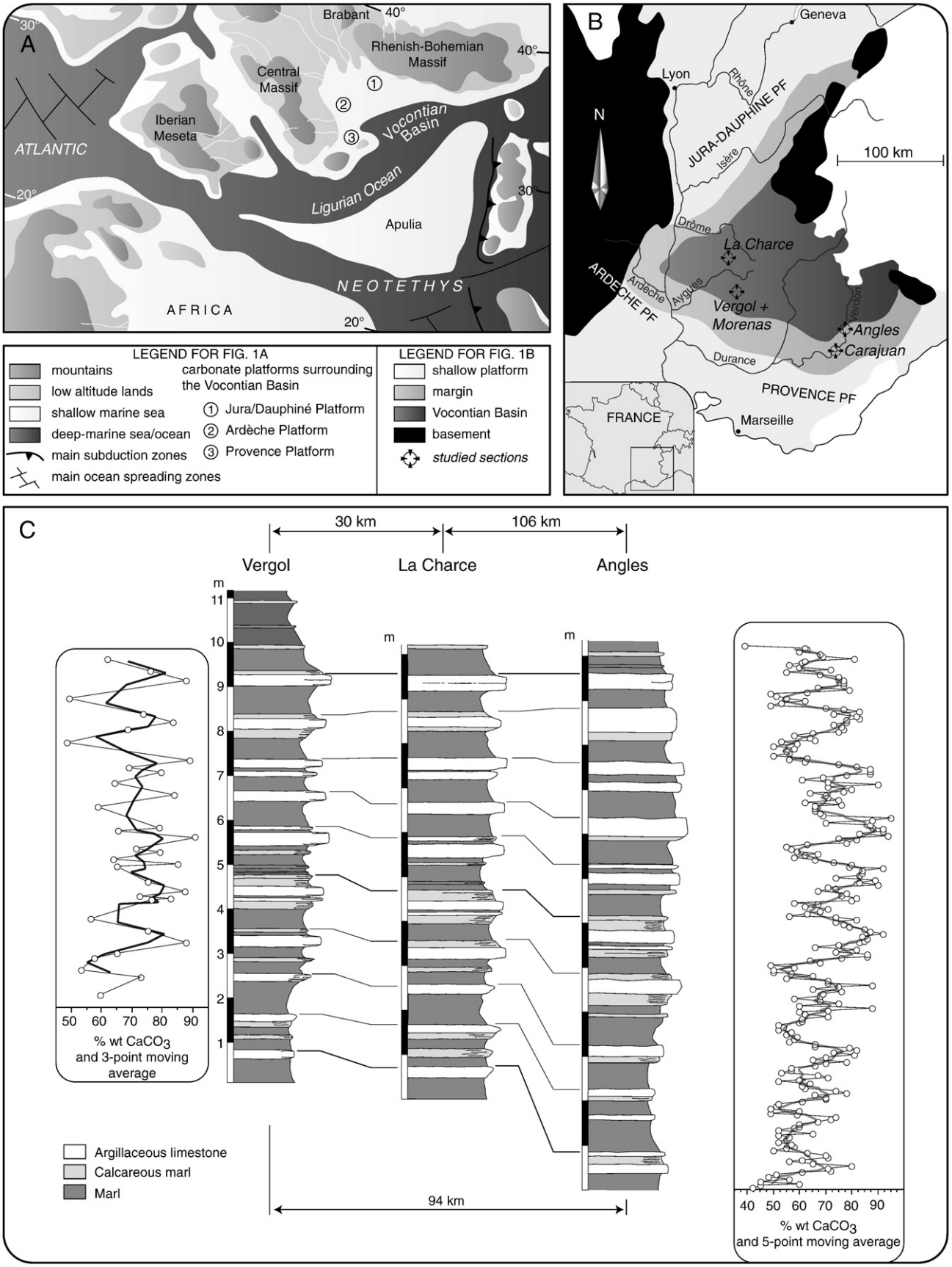

Fig. 1. Location of studied sections in the Vocontian Basin. (A) Paleogeographic reconstruction of the western Tethys and position of carbonate platforms surrounding the basin, after Blakey (2005). The Vocontian Basin opened to the Western Ligurian Tethys ocean to the east (Masse, 1993), and received siliciclastic materials having their source in the Central Massif to the west, possibly in the Corsica–Sardinia to the south, and in the Vosges-Black Forest to the north. (B) Location of studied sections. (C) Bed-to-bed correlations of the calcareous interval "Faisceau médian" in the Vergol, La Charce and Angles sections. Lithology is remarkably similar despite the distance between the sections. Mean cycle thickness is still higher than 1 m as in the whole Upper Valanginian (thicknesses from Giraud et al., 1995).

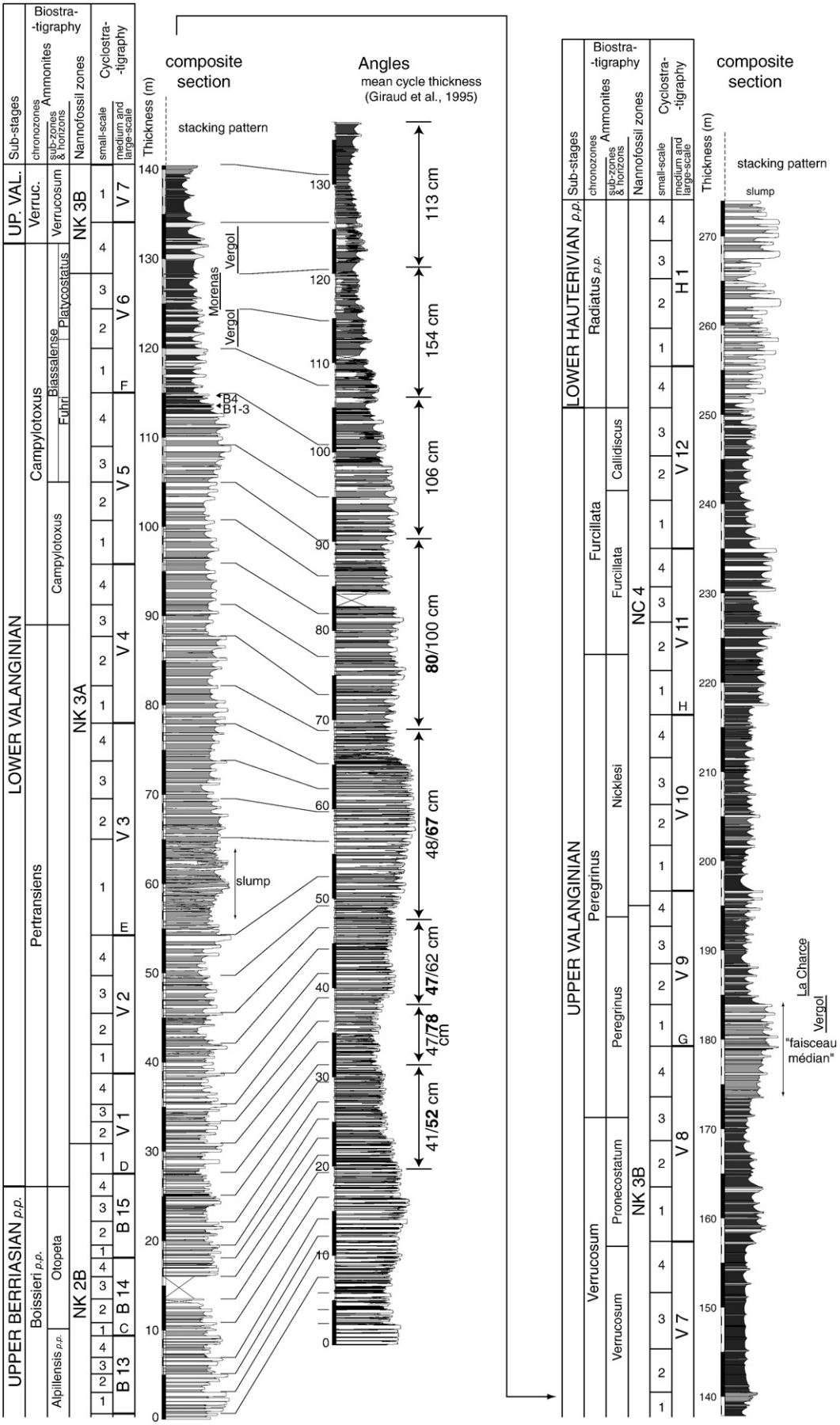

Nannoconus steinmannii steinmannii displays in the samples studied here a length ~25% smaller than that measured by Tremolada and Young (2002), and the 3363.9 pg per specimen given by these authors implies an overestimation of the pelagic carbonate fraction. In order to reduce mass uncertainties of the most important pelagic carbonate producers, the size of 1314 *Nannoconus* specimens in 37 samples was measured in the Vergol and La Charce sections. Mean size of the three most common species, i.e. *Nannoconus steinmannii*, *Nannoconus kamptneri* and *Nannoconus globulus*, were consequently used in volume and mass calculations. Also, a comparable size of *Watznaueria biporta* (a taxon of known mass of 153.9 pg; Bornemann et al., 2003) and *Haquius circumradiatus* has led us to attribute the mass of *W. biporta* to *H. circumradiatus*. The taxa with known masses represent on average 88.9% of the total nannofossil assemblage and include the most bulky species (Table 1).

3.3. Carbonate and clay accumulation rates

Accumulation rates for carbonates and clays were estimated in the same way as the method described above, but for a longer stratigraphic interval, from the uppermost Berriasian (middle Alpillensis Subzone) to the lowermost Hauterivian (Radiatus Zone). Total thickness of marl layers and of limestone beds were calculated within each small- and medium-scale sequence defined by Gréselle and Pittet (2010). Short and medium-term sedimentation rates (i.e., 100 ka and 400 ka) can thus be seen as a good estimate of carbonate and clay accumulation rate, respectively.

3.4. Stable isotope analysis of carbonates

Oxygen and carbon isotope compositions have been measured on 64 carbonate samples, covering the Campylotoxus, Verrucosum and Peregrinus Zones of the Vergol section (Fig. 4). Carbonate powders were reacted with 100% phosphoric acid (density >1.9; Wachter and Hayes, 1985) at 75 °C using a Kiel III online carbonate preparation line connected to a ThermoFinnigan 252 mass-spectrometer in Erlangen. All values are reported in per mil relative to V-PDB by assigning a $\delta^{13}C$ value of +1.95‰ and a $\delta^{18}O$ value of −2.20‰ to NBS19. Reproducibility (1 standard deviation) was checked by replicate analysis of laboratory standards and is better than ±0.03 for $\delta^{13}C$ and ±0.1 for $\delta^{18}O$.

4. Results

4.1. Carbonate content

Stratigraphic changes in carbonate content are well visible when the mean carbonate content per marl–limestone alternation is calculated (thick line and open squares in Fig. 5). At the base of the analyzed interval, mean carbonate content varies between 61 and 78 wt.% $CaCO_3$. A decrease in carbonate content begins some 5 m above the base of the Biassalense Subzone, from around 50–67 wt.% in the uppermost Lower Valanginian to a minimum of ~46 wt.% $CaCO_3$ in the upper part of the Verrucosum Subzone in the Upper Valanginian. Upsection, carbonate content raises again with values of 60–65 wt.% in the Pronecostatum Subzone, and 65–75 wt.% at the base of the Peregrinus Zone. Carbonate contents are around 65 wt.% from the Peregrinus to the Furcillata Subzone. A maximum of 71 wt.% is recorded in the uppermost Furcillata Subzone, whereas the last analyzed marl–limestone alternation has a mean carbonate content of 66 wt.% $CaCO_3$.

4.2. Nannofossil preservation

Nannofossils from the Vergol section are remarkably well-preserved in most of the samples checked under both light and scanning electron microscopes. At La Charce, the preservation is moderate to good. Etching was not observed and in a few samples some large taxa such as *Haquius* showed secondary overgrowth. Tiny and delicate coccoliths, such as representatives of *Zeugrhabdotus* or *Staurolithites* showing pristine central area structures were observed in the studied samples. In some cases, fragmentation of nannofossils was observed. However, entire coccosphaeres were also commonly observed in the studied samples. This record indicates only minor effects of fragmentation affecting nannofossil material. No significant difference in the preservation of the nannofossils occurred between marl and limestone beds, but a slightly poorer preservation was observed in the levels B1, B2 and B3 (Fig. 2), probably related to higher organic-matter contents in this interval.

4.3. Nannofossil abundance and flux

Nannofossil abundance per gram of rock displays both short- and long-term variations along the section (Fig. 3). On short-term scales (at the scale of the marl–limestone alternations), nannofossil abundance is systematically lower in limestones than in marls, with carbonate contents and nannofossil abundances being negatively correlated (Fig. 6). Low nannofossil abundances are observed in five samples in the interval enriched in organic-matter (B1–B4 Barrande layers; Reboulet et al., 2003; Fig. 3). Some other four poorly-preserved samples come from a 5 m-thick stratigraphic interval at the boundary between the Campylotoxus and Biassalense Subzones.

Nannofossil abundance per gram of rock combined with the duration of ~20 kyr for the marl–limestone alternations allows the calculation of nannofossil fluxes to the sediment, measured per square meter and per year. Total nannofossil abundance and flux well mirror the fluctuations of both nannolith and coccolith (Fig. 3). At the base of the studied interval, in the uppermost Campylotoxus and lowermost Biassalense Subzones, mean nannofossil abundances per marl–limestone alternation fluctuate between 0.2 and 0.56 billion specimens per gram of rock. Nannofossil flux is low with mean values per marl–limestone alternations of 40 billions nannofossils $m^{-2}\,yr^{-1}$. A first increase in the nannofossil abundance and flux is recorded close to the base of the Fuhri horizon, with mean abundances of 0.7 to 1.27 billion nannofossils per gram of rock, and mean nannofossil flux of 60 to 156 billions nannofossils $m^{-2}\,yr^{-1}$ in most parts of the Fuhri and Platycostatus horizons, except in the interval containing the B1–B4 Barrande layers that display average abundances of 0.5–0.6 billion nannofossils and the lowest nannofossil fluxes (Fig. 3). An abundance maximum (~2.1 billions specimens per gram of rock) and the highest nannofossil fluxes (372 billions specimens $m^{-2}\,yr^{-1}$) occur a few meters below the Lower/Upper Valanginian boundary. A gradual decrease in the nannofossil abundance (between 0.45 and 1 billion specimens per gram of rock) and fluxes (between 70 and 163 billions $m^{-2}\,yr^{-1}$), even if still high, marks the middle part of the studied section, namely the Peregrinus Subzone (Fig. 3). From the Nicklesi Subzone to the basal Hauterivian (Radiatus Zone), nannofossil abundance and fluxes are quite stable with values between 108 and 154 billions $m^{-2}\,yr^{-1}$.

Fig. 2. Bed-to-bed correlation between Angles and the synthetic basinal section (Vergol, Morenas and La Charce sections). The Standard Ammonite Zonation (Kilian Group, Hoedemaeker et al., 2003; Reboulet et al., 2006, 2009) used here is applied on these sections following the biostratigraphy from Reboulet et al. (1992, 2003), Reboulet (1996), Reboulet and Atrops (1999). These sections are characterized by marl–limestone alternations that are typically carbonate-rich at the base of the Valanginian, becoming gradually clay-richer starting from the organic-matter-rich Barrande layers, in the uppermost Lower Valanginian (B1 to B4; Reboulet et al., 2003). The Upper Valanginian is generally argillaceous except for few intervals where thicker limestone beds occur. Mean cycle thickness are less than 0.5 m in the Alpillensis Subzone and more than 1 m in the uppermost Lower and Upper Valanginian (from Giraud et al., 1995).

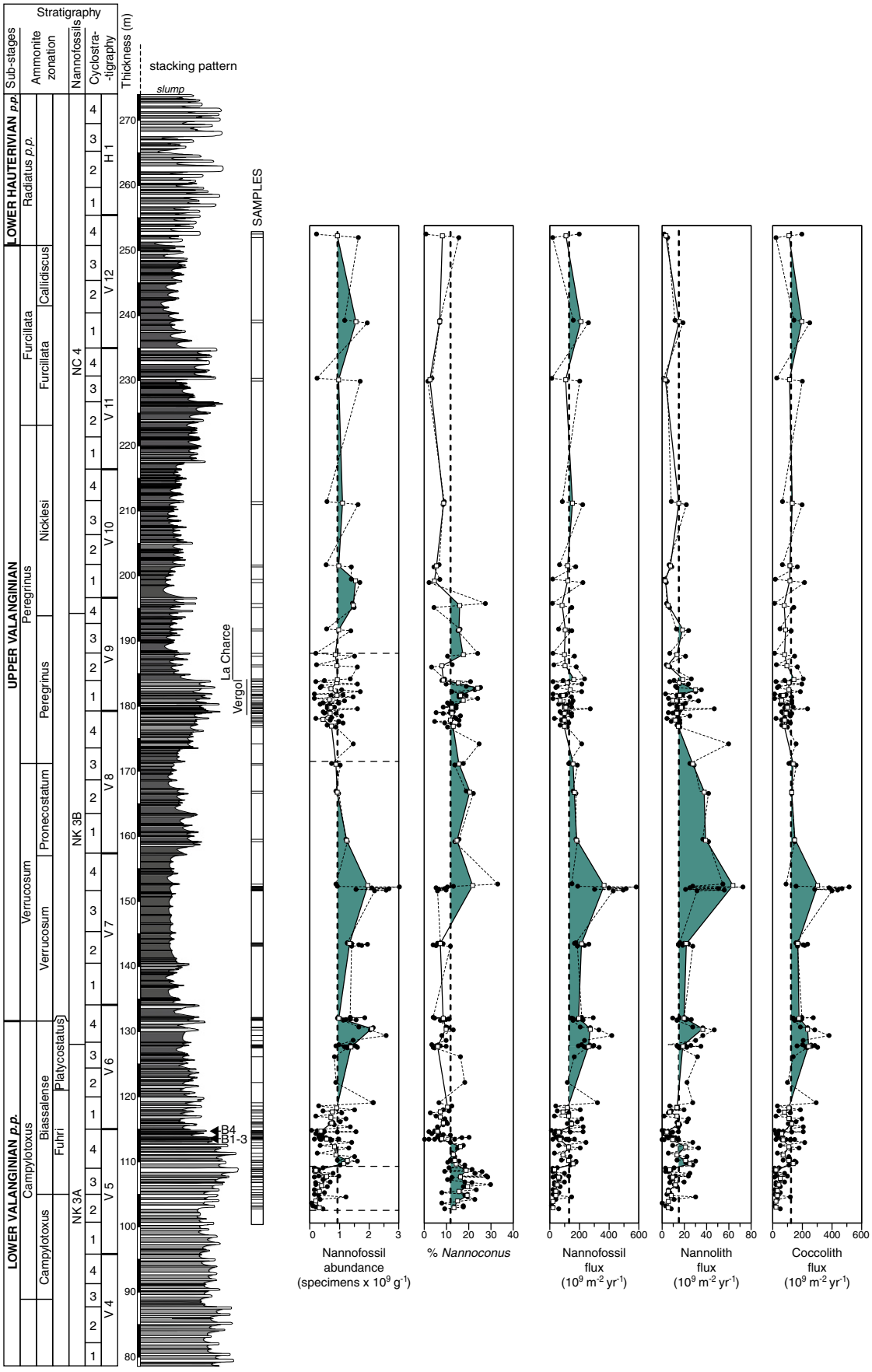

Fig. 3. Evolution of nannofossil abundance and fluxes from the Lower to the uppermost Valanginian along the composite section. Nannofossil fluxes are calculated for nannoliths, coccoliths and total nannofossils. Values strongly vary with lithology, and means for each marl–limestone alternation are indicated by white squares. Gray areas represent evolution above the Valanginian average values indicated by black dotted line. B1 to B4 stand for Barrande layers 1 to 4 (Reboulet et al., 2003).

Table 1
List of taxa in analyzed samples and corresponding masses, and mean taxa percentages of both known and unknown mass.

List of taxa present in the analyzed samples	Mass in picograms				Mean% of nannofossils of known mass in the studied samples	Mean% of nannofossils of unknown mass in the studied samples	Remarks
	Tremolada and Young (2002)	Erba and Tremolada (2004)	Bornemann et al. (2003)	This study			
Anfractus harrisonii						0.443	
Assipetra infracretacea	95.5	96	95.6	95.5	0.002		
Biscutum constans/ellipticum	8.5	8.6	3.5	3.5	1.493		
Calcicalathina oblongata			519.5	519.5	0.249		
Calculites sp 1					0.037		
Conusphaera mexicana mexicana			149.3	149.5	0.031		
Conusphaera mexicana minor			22.4	22.4	0.083		
Conusphaera rothii						0.175	
Cretarhabdus/Retecapsa spp.			84.9	84.9	1.701		
Cribropshaerella ehrembergi						0.018	
Crucibiscutum salebrosum						0.042	
Cruciellipsis cuvillieri			133.1	133.1	1.482		
Cyclagelosphaera margerelii			6.5	6.5	6.203		
Cyclagelosphaera rotaclypeata						0.527	
Diazomatolithus cf. D. lehmanii						0.618	
Diazomatolithus lehmanii		13.8	8.1	8.1	3.127		
Discorhabdus rotatorius/ignotus	10.7	10.8	4.1	4.1	0.675		
Eiffellithus primus						0.046	
Eiffellithus sp.						0.007	
Eiffellithus windii						0.034	
Ethmorhabdus hauterivianus						0.184	
Ethmorhabdus sp. ind.						0.19	
Haquius circumradiatus					1.812		Mass of *W. biporta*
Haquius ellipticus						0.015	
Haquius noeliae						0.005	
Helenia chiastia						0.007	
Kokia borealis						0.006	
Litraphidites carniolensis						0.105	
Loxolitus armilla						0.004	
Manivitella pemmatoidea	102.1	103	.	102.1	0.025		
Micrantholithus hoschulzii	424.2	424	.	424	0.616		
Micrantholitus obtusus						0.074	
Microstaurius chiastus						0.001	
Nannoconus bermudezii						0.018	
Nannoconus boneti						0.007	
Nannoconus broennimanni						0.268	
Nannoconus colomii						0.261	
Nannoconus cornuta						0.033	
Nannoconus dolomiticus			623.7	623.7	0.072		
Nannoconus globulus		2241.4	.	1030	1.324		Undifferentiated in this study
Nannoconus globulus minor							
Nannoconus kamptneri				640	0.482		Undifferentiated in this study
Nannoconus kamptneri minor			456.6				
Nannoconus oviformis						0.03	
Nannoconus quadratus						0.014	
Nannoconus steinmannii minor	770.3	.	496	610	9.384		Undifferentiated in this study
Nannoconus steinmannii steinmannii	3363.9	3363.9	.				
Parhabdolithtus embergeri sp. 2	.	.	750.3	750.3	0.584		
Percivalia fenestrata						0.004	
Rhagodiscus achylostaurion						0.095	
Rhagodiscus angustus						0.077	
Rhagodiscus asper	38.8	39	18.1	18.1	2.377		
Rhagodiscus dekaeneli						0.267	
Rhagodiscus gallagheri						0.479	
Rhagodiscus infinitus						0.006	
Rhagodiscus parallelus						0.055	
Rhagodiscus pseudoangustus						0.363	
Rhagodiscus sp.						0.388	
Rhagodiscus splendens						0.133	
Rotelapillus lafittei						0.01	
Rucinolithus sp.						0.111	
Rucinolithus terebrodentarius youngii	728.8	729	.	728.8	1.648		
Rucinolithus wisei						0.227	
Sollasites horticus						0.001	
Speetonia colligata						0.045	
Staurolithites crux						0.953	
Staurolithites mitchneneri						0.001	

(continued on next page)

Table 1 (*continued*)

List of taxa present in the analyzed samples	Mass in picograms				Mean% of nannofossils of known mass in the studied samples	Mean% of nannofossils of unknown mass in the studied samples	Remarks
	Tremolada and Young (2002)	Erba and Tremolada (2004)	Bornemann et al. (2003)	This study			
Staurolithites mutterlosei						0.116	
Staurolithites sp.						0.182	
Tegumentum stradneri						0.005	
Thoracosphaera eichstaettensis						0.002	
Thoracosphaera sp.						0.031	
Tubidiscus sp.1						0.027	
Tubodiscus jurapelagicus						0.053	
Tubodiscus verenae	.	.	744.8	744.8	0.056		
Umbria granulosa						0.146	
Watznaueria barnesae	55.8	57	72.6	55.8	43.33		
Watznaueria biporta			153.9	153.9	0.464		
Watznaueria britannica			69.1	69.1	2.396		
Watznaueria communis						0.915	
Watznaueria fossacincta			35.1	35.1	6.902		
Watznaueria manivitae			276.5	276.5	0.647		
Watznaueria ovata			15.9	15.9	1.014		
Zeugrhabdotus diplogrammus	25.1	25	.	25	0.053		
Zeugrhabdotus erectus	2.1	2.2	4.5	2.1	0.586		
Zeugrhabdotus fissus						0.004	
Zeugrhabdotus noeliae						0.027	
Zeugrhabdotus sp.						0.152	
Zeugrhabdotus trivectis						0.018	
Zeugrhabdotus xenotus						0.06	
Unidentified taxa						3.06	
				Total percentage	88.855	11.145	

The increase in nannofossil abundance in the Fuhri horizon corresponds also to a higher contribution of nannoliths (mainly nannoconids and *Rucinolithus*; Fig. 3). Consequently, the decrease in the percentage of *Nannoconus* resulted rather from a more effective increase in coccolith abundance than from a decreasing nannolith abundance, in a period of overall increase in the quantities of both groups (Fig. 3).

4.4. Accumulation rates of pelagic, non-pelagic carbonates and of clays based on nannofossil flux

The accumulation rate of pelagic carbonates (expressed as μm yr^{-1}; Fig. 5) was estimated by combining the nannofossil flux and species-specific volumes of the different nannofossil taxa (Table 1). Since accumulation rates are not constant passing form marls to limestones, a mean accumulation rate of pelagic carbonates per marl–limestone alternation was calculated (thick line and open squares; Fig. 5). As nannoliths are among the largest taxa (especially nannoconids; Table 1) pelagic carbonate accumulation rate parallels nannolith absolute abundance and flux (Figs. 3 and 5). An increase in pelagic accumulation rate from 1.7–6 to 3.8–8 μm yr^{-1} is recorded in the Fuhri horizon, and coincides to higher absolute abundances of nannoliths and coccoliths. As the interval containing the B4 Barrande layer recorded the lowest nannolith abundance, accumulation rate of pelagic carbonates also decreases to 2.2 μm yr^{-1} (Reboulet et al., 2003; Figs. 4 and 6). In the Platycostatus horizon and at the base of the Verrucosum Subzone, pelagic carbonate accumulation rate is 7.3 to 16.4 μm yr^{-1}. The uppermost part of the Verrucosum and the Pronecostatum Subzones record the highest accumulation rates of pelagic carbonates with a maximum value of 19.3 μm yr^{-1} (Fig. 5). The interval from the Faisceau médian (Peregrinus Subzone) to the base of the Hauterivian (Radiatus Zone) represents a minimum pelagic carbonate accumulation rate, with values ranging from 2.2 to 5.5 μm yr^{-1}.

Non-pelagic carbonate accumulation rates are generally high in the Lower Valanginian, fluctuating between 22 and 32 μm yr^{-1} (Fig. 5). The lowest accumulation rates between 18.7 and 27.1 μm yr^{-1} are recorded across the Lower/Upper Valanginian boundary. Accumulation rate of non-pelagic carbonates in the Faisceau médian is comparable to that recorded at the base of studied interval, with high values between 25.1 and 35.2 μm yr^{-1}. A second minimum of non-pelagic carbonate accumulation, with values lower than 25 μm yr^{-1}, is recorded up to the base of the Nicklesi Subzone (Fig. 5). Stable rates around 28 m^{-2} yr^{-1} are recorded up to the base of Hauterivian.

Mean clay accumulation rate of marl–limestone alternations varies between 12.7 and 18.6 μm yr^{-1} in the first ten analyzed alternations (Fig. 5). A sharp increase in clay accumulation rate occurs 2 m below the Barrande layers and a maximum rate of 23.9 μm yr^{-1} is recorded in B1–B3 Barrande layers (Fuhri horizon). To the base of the Peregrinus Subzone, clay accumulation rate was between 20.7 and 30.2 μm yr^{-1} (Fig. 5). In the carbonate-rich Faisceau médian, clay accumulation rate decreases between 10.8 and 18.1 μm yr^{-1}. Above this interval and up to the basal Hauterivian, clay accumulation rate is remarkably stable at 15.5 μm yr^{-1} with the exception of a maximum of 22.4 μm yr^{-1} at the base of the Nicklesi Subzone (Fig. 5).

4.5. Accumulation rates of carbonate and clay based on bed thickness

Carbonate and clay accumulation rates were calculated for each short- and medium-term sequence (having an average duration of 100 and 400 kyr, respectively; Fig. 4). Total accumulation rate generally increases in the Biassalense and Verrucosum Subzones, and progressively decreases up to the base of the Hauterivian. Conversely, carbonate accumulation rate shows an inverse trend with a progressive decrease up to the Peregrinus Subzone and a gradual increase up to the uppermost Valanginian (Fig. 4). From the base of the Campylotoxus Zone to the Barrande layers, the increase in total accumulation rate is linked to a raise in carbonate accumulation

Fig. 4. Evolution of accumulation rates for carbonate beds and marly intervals, oxygen and carbon stable isotopes. For carbonate beds, marly intervals and total accumulation rates, both short-term (100 kyr) and medium-term (400 kyr) evolution are represented respectively by dots and squares. Isotopic data from the uppermost Peregrinus Subzone to the Hauterivian are from Hennig et al. (1999; triangles). B1 to B4 indicate the Barrande layers 1 to 4 (Reboulet et al., 2003).

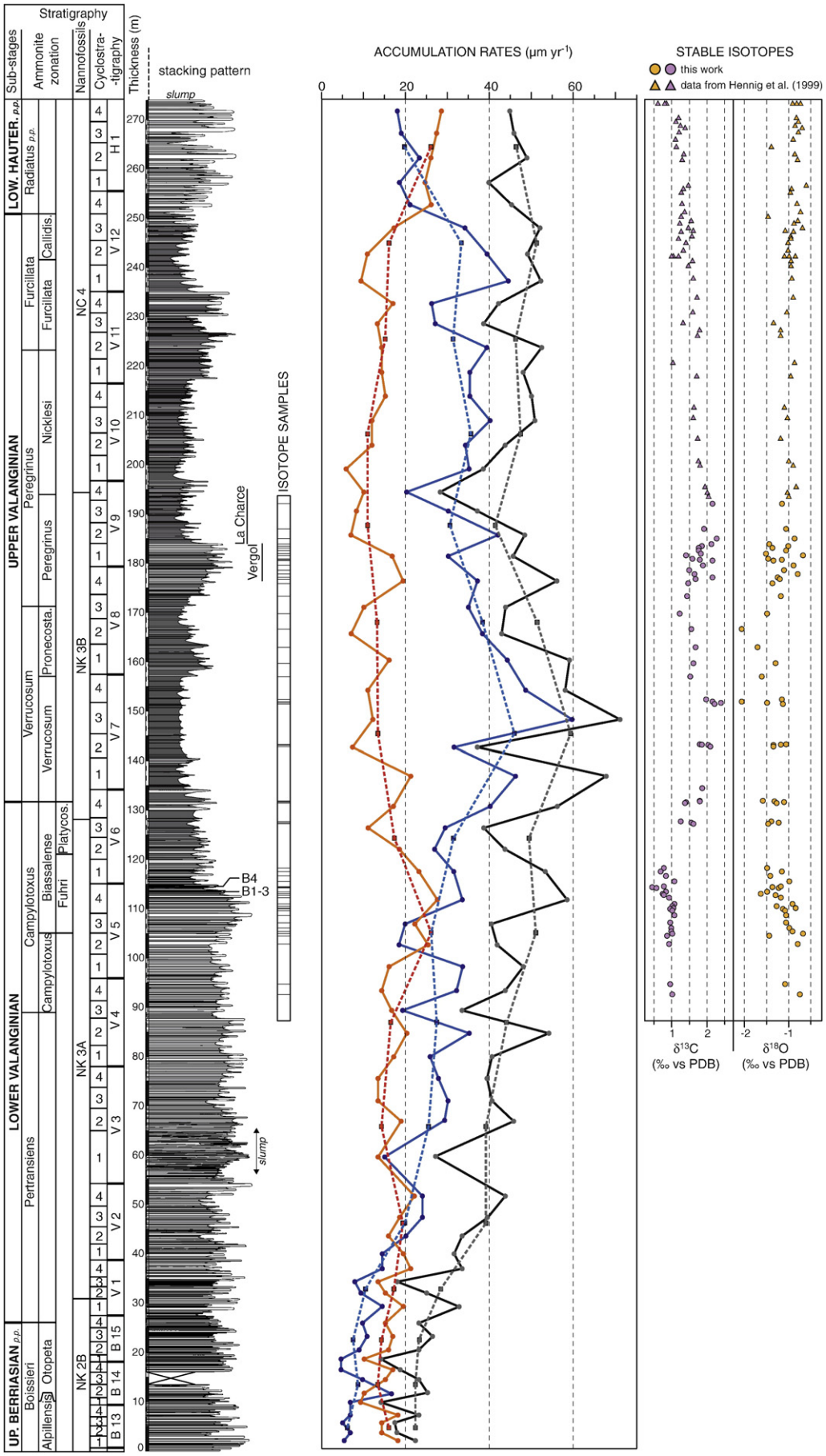

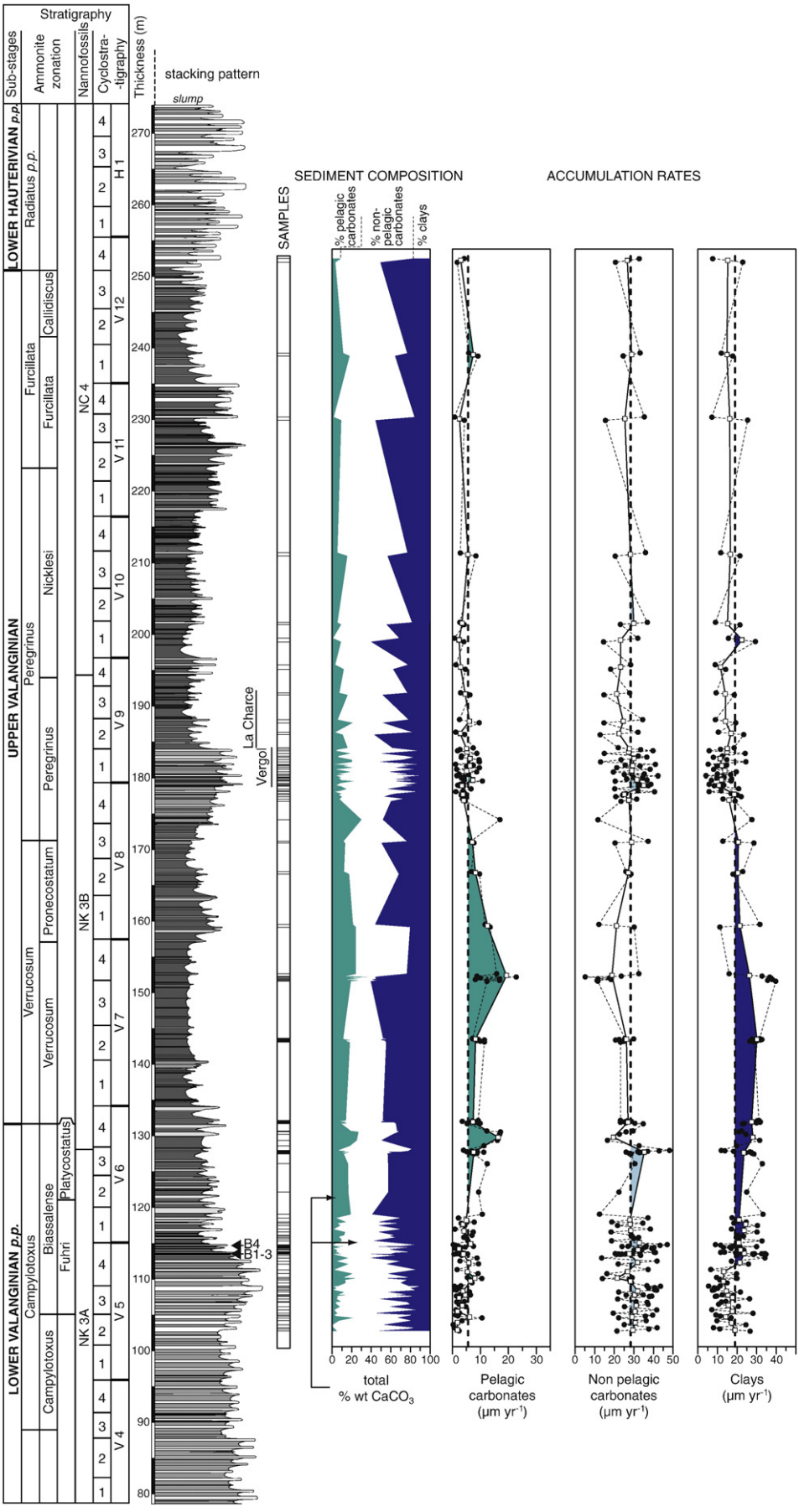

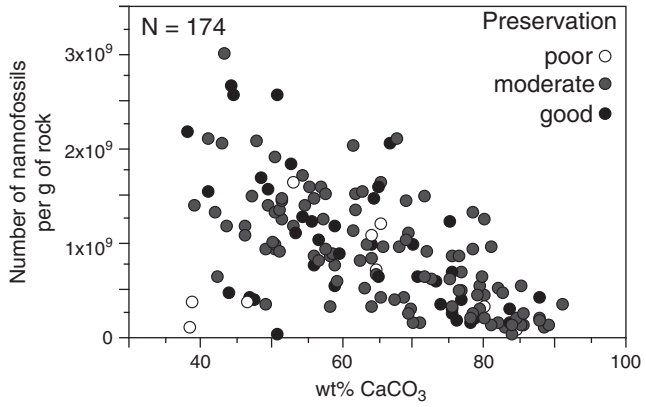

Fig. 6. Correlation between carbonate content and absolute nannofossil abundance.

from 17 to 25 μm yr^{-1}, whereas marl accumulation rates are rather stable around 23 μm yr^{-1}. From this interval to the first thick Hauterivian carbonate beds, marl and total sediment accumulation rate covary (Fig. 4). A sharp increase in total sediment accumulation rate to a maximum of 59 μm yr^{-1} in the Verrucosum Subzone corresponds to an increase in the marl accumulation rate from 26 to 46 μm yr^{-1}. A progressive decrease in accumulation rates from Verrucosum to the base of the Nicklesi subzones is only interrupted by a short-term maximum in the carbonate accumulation rate at 19 μm yr^{-1} in the carbonate-rich Faisceau médian (Fig. 4). Upsection, the bulk sediment is still mainly composed of argillaceous marls in this interval. Carbonate accumulation rate slowly increases up to 12 μm yr^{-1} just below the carbonate-rich basal Hauterivian while clay accumulation rate fluctuates between 26 and 44 μm yr^{-1}. The uppermost Valanginian (Callidiscus Subzone) and the lowermost Hauterivian (Radiatus Zone) are marked by a sharp increase of carbonate accumulation rate from 12 to 27 μm yr^{-1} (Fig. 4).

4.6. Carbon and oxygen isotopes

The Vergol section records the positive carbon isotope excursion (McArthur et al., 2007; this work, Fig. 4) typically recorded in the Lower/Upper Valanginian transition worldwide (Cotillon and Rio, 1984; Lini et al., 1992; Channell et al., 1993; Föllmi et al., 1994; Hennig et al., 1999; van de Schootbrugge et al., 2000; Wortmann and Weissert, 2000; Adatte et al., 2001; Bartolini, 2003; Erba et al., 2004; Price and Mutterlose, 2004; Gröcke et al., 2005; Sprovieri et al., 2006; Duchamp-Alphonse et al., 2007; Bornemann and Mutterlose, 2008). Bulk rock carbon isotopes present values of about 1‰ in the Campylotoxus Subzone, that increase up to ~2.4‰ in the upper part of the Verrucosum Subzone after an initial negative excursion of about 0.5% in the Barrande layers (B4; Fuhri horizon; Fig. 4). In the uppermost Verrucosum to Pronecostatum subzones, carbon isotope ratios decline to values between 1.3 and 1.6‰ and fluctuate between 1.5 and 2.3‰ in the Peregrinus Subzone. Comparable carbon isotope records were measured in the Angles section of the Vocontian Basin (Fig. 7; Duchamp-Alphonse et al., 2007), and at the Provence Platform Margin (Carajuan section; Hennig et al., 1999). This event is synchronous in all these sections as indicated by their good biostratigraphic and sequence stratigraphic control (Reboulet and Atrops, 1995, Reboulet et al., 2003; Gréselle and Pittet, 2010). Interestingly, the minor negative carbon isotope shift preceding the Valanginian positive excursion is recorded in all three sites, and coincides in Vergol to the interval containing the fourth organic-matter-rich Barrande layer (Reboulet et al., 2003; B1–B4 in Figs. 2 and 4).

Oxygen isotopes show a trend toward lighter values from the Campylotoxus (−0.7 to −1.2‰) to the Biassalense (−1 to −1.7‰) subzones. Oxygen isotope values remain stable up to the upper part of the Verrucosum Subzone where one sample displays a $\delta^{18}O$ value of ~−2.1‰ (Fig. 4). A decrease of $\delta^{18}O$ values is then recorded up to the middle part of the Pronecostatum Subzone where $\delta^{18}O$ values reach −2.1‰. From there, $\delta^{18}O$ increases again up to values between −0.7 and −1.5‰ during the Peregrinus Subzone.

5. Discussion

5.1. Origin of the carbonate mud in the studied sediments

The Vergol and La Charce sections in the Vocontian Basin show spectacular marl–limestone alternation, in which calcareous nannofossils are important contributors to the carbonate fraction. Three hypotheses exist to explain the formation of marl–limestone alternations, which involve either primary fluctuations (1) of clay (e.g., Einsele and Ricken, 1991; Elder et al., 1994; Laurin and Ulicny, 2004), (2) of carbonate accumulation in the basin, or (3) a diagenetic redistribution of carbonate within the sediment (e.g., Eder, 1982; Ricken, 1986; Munnecke and Samtleben, 1996; Munnecke et al., 2001). Carbonate fluctuations may result either from changes in pelagic carbonate accumulation (e.g., Cotillon et al., 1980; Ricken, 1994; Einsele, 2000), or from changes in accumulation of carbonates produced on the platform and exported basinwards (e.g., Droxler and Schlager, 1985; Reijmer et al., 1988; Schlager et al., 1994; Pittet and Strasser, 1998; Betzler et al., 1999; Rendle-Bühring and Reijmer, 2005).

The Valanginian marl–limestone alternations of the Vocontian Basin can be correlated bed-by-bed at a 100 km-scale (Cotillon et al., 1980; Ferry, 1991; Figs. 1 and 2). Also, these alternations have likely formed in tune with changes in the Earth's orbital parameters (Giraud et al., 1995; Gréselle and Pittet, 2010). Consequently, a diagenetic origin of the limestone–marl alternations studied here can be excluded. Calcareous nannofossil abundance (Fig. 3), as well as the pelagic carbonate fraction, is lower in the limestones than in the marls (Fig. 5). This pattern cannot be related to a differential preservation in the two lithotypes as nannofossil preservation is comparable. As a consequence, preservation of calcareous nannofossils was not responsible for the fluctuations in carbonate content, and for the formation of the marl–limestone alternations, as already proposed for part of the studied interval (23.5–31 m in Fig. 2) by Reboulet et al. (2003). Changes in clay input are unlikely to have formed the observed marl–limestone alternations since the resulting higher dilution should have led to a lower quantity of nannofossils in marls. Instead, calcareous nannofossils and organic-matter content (Reboulet et al., 2003), are systematically more abundant in marls than in limestones and, in some clay-rich samples, nannofossil-derived carbonate forms the entire carbonate fraction (Fig. 5).

This study shows that the Valanginian marl–limestone alternations of the Vocontian Basin resulted from changes in the amount of platform-derived carbonate mud shed into the basin. Reboulet et al. (2003) have shown that the main phases of carbonate accumulation at the margin of the Provence Platform (to the south of the Vocontian Basin; Fig. 1) are contemporaneous to the main phases of carbonate deposition in the basin. The Provence Platform margin had a ramp-morphology, and sea-level fluctuations controlled the distal-to-proximal migration of facies belts from offshore to shoreface environments (Gréselle and Pittet, 2010). These changes resulted in the deposition of marl-dominated

Fig. 5. Evolution of sediment composition and accumulation rates of different sedimentary component. Sediment percentage and accumulation rates were calculated for pelagic and non-pelagic carbonates as well as for clays. Values might strongly differ with lithology and means for each marl–limestone alternation are indicated by white squares. Gray areas represent evolution above the Valanginian mean indicated by black dotted line. B1 to B4 indicate the Barrande layers 1 to 4 (Reboulet et al., 2003).

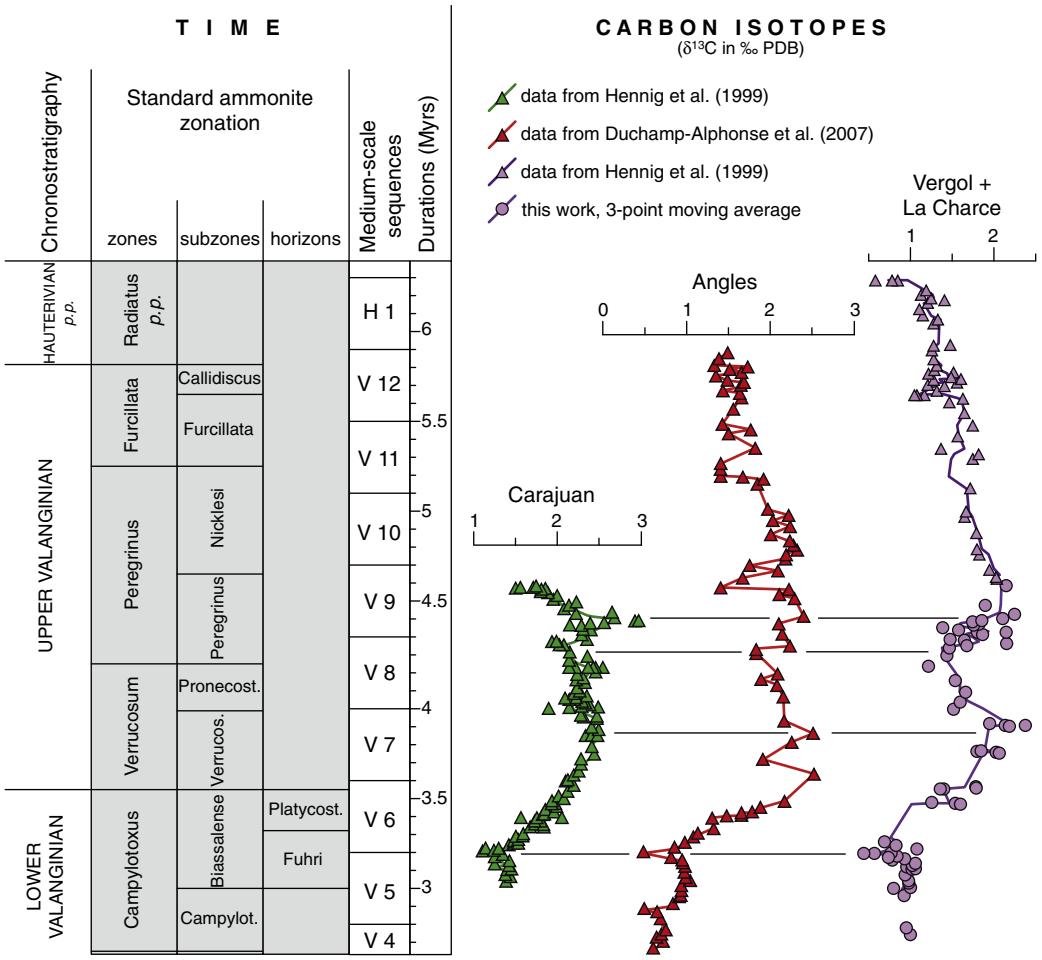

Fig. 7. Correlation between carbon isotope signal from Carajuan (margin of the Provence Platform), Angles, Vergol and La Charce sections. Data for Carajuan and La Charce from Hennig et al. (1999). Carbon isotope data for Angles from Duchamp-Alphonse et al. (2007). General trends are remarkably similar with a small-amplitude negative excursion in the Biassalense Subzone and two positive shifts in the Verrucosum and Peregrinus subzones.

facies offshore, and carbonate-dominated shoreface (Reboulet et al., 2003). This pattern suggests that changes in carbonate content in the basin mainly resulted in fluctuations of the export intensity of platform-derived carbonate mud, occurring both on the long-term (3rd-order transgressive–regressive trends) and on the short-term (marl–limestone alternations). At the scale of the marl–limestone alternations, the imported platform-derived mud diluted the parauthochtonous nannofossil quantities, explaining lower nannofossil abundances in limestones with respect to marls. Changes in nannofossil fluxes in the marl–limestone alternations of the Vocontian Basin can therefore be used as a proxy for reconstructing platform-derived carbonate fluxes and, ultimately, to assess the relationships between platform and basin evolution in times of environmental perturbations.

5.2. Duration of the Weissert Event

The Valanginian recorded a series of palaeoenvironmental perturbations showing a peculiar timing with respect to the $\delta^{13}C$ positive excursion. The Weissert Event started in the uppermost Lower Valanginian (Biassalense Subzone, Fuhri horizon; McArthur et al., 2007; Fig. 4) and pre-excursion values are recorded again near the Lower/Upper Hauterivian boundary (Sprovieri et al., 2006), giving a total duration of approximately 5 Myr for this event, based on the cyclostratigraphic framework of Gréselle and Pittet (2010). This duration is in agreement with that proposed by Sprovieri et al. (2006) who identified 11.5 cycles of 400 kyr-eccentricity or 2.2 cycles of 2400 kyr-eccentricity for this interval, although the duration estimated for the rise of the carbon isotopic values is shorter in the present work (1.5 Myr) than the 2.3 Myr proposed by Sprovieri et al. (2006).

5.3. Palaeoenvironmental changes during the Weissert Event

The $\delta^{13}C$ record shows four major phases: (i) rather stable, pre-excursion values ending with a 0.5‰ negative spike, (ii) a 2‰ rise to form the first positive maximum, (iii) a 1‰ decrease followed by the second maximum and, (iv) a long-term decrease in $\delta^{13}C$ to pre-excursion values (Figs. 4, 7 and 8). From the Berriasian/Valanginian boundary to the base of the Fuhri horizon, when carbon isotope values are quite stable (Emmanuel and Renard, 1993; this work), both clay and carbonate fluxes rise (Fig. 8). The decrease in the relative abundance of *Nannoconus* from about 30% to less than 10% in the Fuhri horizon corresponds to the onset of the "Nannoconid decline" defined by Bersezio et al. (2002). Similarly, an important decrease in nannoconids has been reported in Italy (Erba and Tremolada, 2004), and a decline in the Western Atlantic (Bornemann and Mutterlose, 2008).

The increase of carbonate accumulation rate is probably due to the long-term progradation and highstand-shedding of the Jura-Dauphinois Platform to the North (Gréselle and Pittet, 2010). The long-term increase of clay flux is twice as important than the carbonate input. A sharp increase in clay influx began 100 kyr after the onset of Nannoconid decline, i.e. 20 kyr before the deposition of the first Barrande layer (Fig. 5). This represents an acceleration of a longer-term increase in clay accumulation rate that began near the Berriasian/Valanginian boundary. The clay influx tripled in 3.5 Myr,

up to its maximum in the Verrucosum Subzone (Fig. 8). Given its time-duration, the major increase in clay accumulation rate may be related to an intensification of continental weathering and runoff of the mountain ranges surrounding the Vocontian Basin, and subsequent clay shedding basinwards.

The deposition of the Barrande layers (Fuhri horizon) parallels the decrease in the nannofossil flux and in the $\delta^{13}C$ values, implying a strongly reduced productivity as less ^{12}C is incorporated in organic-matter (Scholle and Arthur, 1980; Arthur et al., 1987). These levels may have formed under anoxic conditions (Reboulet et al., 2003; Westermann et al., 2010). The lowest $\delta^{13}C$ values are reached during the deposition of the fourth Barrande layer, simultaneously with a minimum abundance of calcareous nannofossils. The negative $\delta^{13}C$ excursion is recorded during a major sea-level lowstand when the Jura-Dauphinois Platform was exposed during more than 400 kyr (Gréselle and Pittet, 2010; Fig. 8). Given the specific physiography of the Vocontian Basin with an oceanic opening only to the East (Fig. 1), the sea-level fall in the Fuhri horizon could have triggered a sluggish oceanic circulation and slowed down water mixing, thus favoring water column stratification and the deposition of the organic-matter-rich Barrande layers (Reboulet et al., 2003) in dysaerobic sea-bottom conditions (Westermann et al., 2010).

From the Barrande layers upsection, the accumulation rate of non-pelagic, platform-derived carbonates decreased and it was generally low during the Late Valanginian (Figs. 4, 5 and 8). Up to the latest Valanginian, the Jura-Dauphinois platform-top was exposed most of the time, and shallow-water carbonate production was limited to marginal areas and therefore strongly reduced (Gréselle and Pittet, 2010; Fig. 8). In addition, the Barrande layers mark the synchronous increase of the calcareous nannofossil flux, especially coccoliths, of the clay influx and the onset of the positive $\delta^{13}C$ positive excursion (Fig. 8). These higher fluxes of coccoliths and clay suggest an increased productivity stimulated by higher levels of continent-derived nutrients. Higher continent weathering rates during the Late Valanginian (McArthur et al., 2007), and particularly across the Early/Late Valanginian boundary, have indeed been inferred. A higher coccolithophorid production across the Early/Late Valanginian boundary is consistent with higher productivity in several oceanic sites, as suggested by higher Sr/Ca ratios (Stoll and Schrag, 2001). Furthermore, the occurrence of high-fertility coccolith taxa is reported by various authors for this interval (Erba et al., 2004; Erba and Tremolada, 2004; Duchamp-Alphonse et al., 2007; Bornemann and Mutterlose, 2008). Higher fertility of marine waters at that time is also suggested by higher phosphorus accumulation rate as reported in the Helvetic (Föllmi, 1995; van de Schootbrugge et al., 2003) and in Carpathians realms (Krobicki and Wierzbowski, 1996).

This higher nutrient input is remarkably synchronous with a change in carbonate producers on the Jura-Dauphinois Platform. Whereas phototrophic producers (coralgal assemblages) formed a flat-topped platform prior to its exposure, carbonates of the Upper Valanginian Bourget Formation were produced only by heterozoans on a carbonate ramp (bryomol facies; Gréselle and Pittet, 2010). This transition corresponds to a change from a 'tropical carbonate factory' (T factory) to a 'cool-water carbonate factory' (C factory) following the classification of Schlager (2000, 2003). Similar changes of carbonate platform producers were observed in other Tethyan and Atlantic platforms (Funk et al., 1993; Föllmi, 1996; Föllmi et al., 2006), and generally preceded their demise (Masse and Philip, 1981; Schlager, 1981; Harris et al., 1984; Föllmi et al., 1994; Weissert et al., 1998). Demise of several platforms, as well as the change of carbonate producers observed on the Jura-Dauphinois Platform illustrate the general drop of platform productivity and the resulting decrease in carbonate mud export toward the Vocontian Basin.

This enhanced nutrient influx is therefore recorded synchronously in the Jura-Dauphinois Platform and in the Vocontian Basin. The platform and pelagic carbonate productions reacted, however, in an opposite way. The maximum nannofossil abundance is contemporaneous with maximum clay input, minimum platform-derived carbonate flux, and the first positive peak in $\delta^{13}C$ (Figs. 3, 5 and 8). The first part of the positive $\delta^{13}C$ excursion is most probably linked to a higher primary productivity in the basin stimulated by high nutrient concentrations.

The decrease in $\delta^{13}C$ following the first peak corresponds to a decreased pelagic carbonate production in a context of cooler marine temperatures (McArthur et al., 2007; Fig. 8). In parallel, a higher input of platform-derived carbonates, as illustrated by the occurrence of the carbonate-rich sediments of the Faisceau median, is linked to a shorter transport distance from shallow-water areas as consequence of sea-level lowering (Gréselle and Pittet, 2010; Fig. 8). The second $\delta^{13}C$ peak occurred concomitant with the lowest temperatures of the Valanginian (Pucéat et al., 2003; McArthur et al., 2007; Fig. 8). The pelagic carbonate production continuously decreased from the first $\delta^{13}C$ peak, in the Verrucosum Subzone, to the Nicklesi Subzone, i.e. after the second carbon isotope peak (Fig. 8). Contrarily to the first peak, no correlation is observed between the increase in carbon isotope values in the Peregrinus Subzone and the nannofossil abundance. The second positive $\delta^{13}C$ peak of the Weissert Event is here tentatively interpreted as being related to high primary productivity supported by non-calcifying organisms.

The start of the $\delta^{13}C$ decrease occurred 1 Myr earlier than the significant rise of platform-derived carbonate input documented by the thick Hauterivian calcareous beds (Fig. 8). From the base of the Nicklesi Subzone to the earliest Hauterivian, $\delta^{13}C$ continuously decreased whereas no noticeable change is recorded in the pelagic carbonate flux. However, the clay input is still high from the Faisceau médian to the lowermost Hauterivian, whereas the non-pelagic carbonate flux remains low (Fig. 8). The reduced carbonate export from shallow-water platforms suggests that these latter have not yet recovered from the crisis, probably because of rapid and high-amplitude sea-level changes (Gréselle and Pittet, 2010; Fig. 8).

5.4. Comparison of nannofossil fluxes with previous work and climate interpretation

Erba and Tremolada (2004) present nannofossil fluxes for the Polaveno section located in the Lombardy Basin, Southern Alps. Although their method of quantification differs from the one used here, some comparisons of fluxes calculated in the Vocontian Basin and Lombardy Basin can be done. The nannofossil fluxes measured in the Lombardy Basin are generally slightly lower than those measured in the Vocontian Basin, although in the same order of magnitude. Interestingly, during the Nannoconid decline fluxes decreased form 7–8 μm/an to less than 4 μm/an in the Lombardy Basin, whilst they increased from average values of 5 μm/an to 10 μm/an in the Vocontian Basin (Fig. 8). This discrepancy can be interpreted in terms of different paleoceanographic conditions occurring in the two basins located at different paleolatitudes.

The progressive, then sharp increase in clay influx in the Vocontian Basin illustrates an increase in continental weathering and run-off probably triggered by a long-term climate change during the Valanginian. This climate change toward more humid conditions may have been triggered by enhanced greenhouse conditions following the volcanic activity of the Paraña–Etendeka province as suggested by Erba et al. (2004), Weissert and Erba (2004), Peate (2009) and Zhu et al. (2009). However, a great uncertainty in the absolute ages of this volcanic activity remains, and its link with the carbon isotope excursion characterizing the Valanginian Weissert Event is not unambiguously proven (McArthur et al., 2007; Thiede and Vasconcelos, 2010). Alternatively, the climatic change toward more humid conditions and related increase in clay accumulation in the basin may be associated with a migration of latitudinal climatic belts. A global climatic change is suggested by a Late Valanginian cooling event recorded in the Vocontian Basin (Pucéat et al., 2003; McArthur et al., 2007), in northern Germany (Podlaha et al., 1998), in western Siberia (Price and Mutterlose, 2004) and in the Arctic

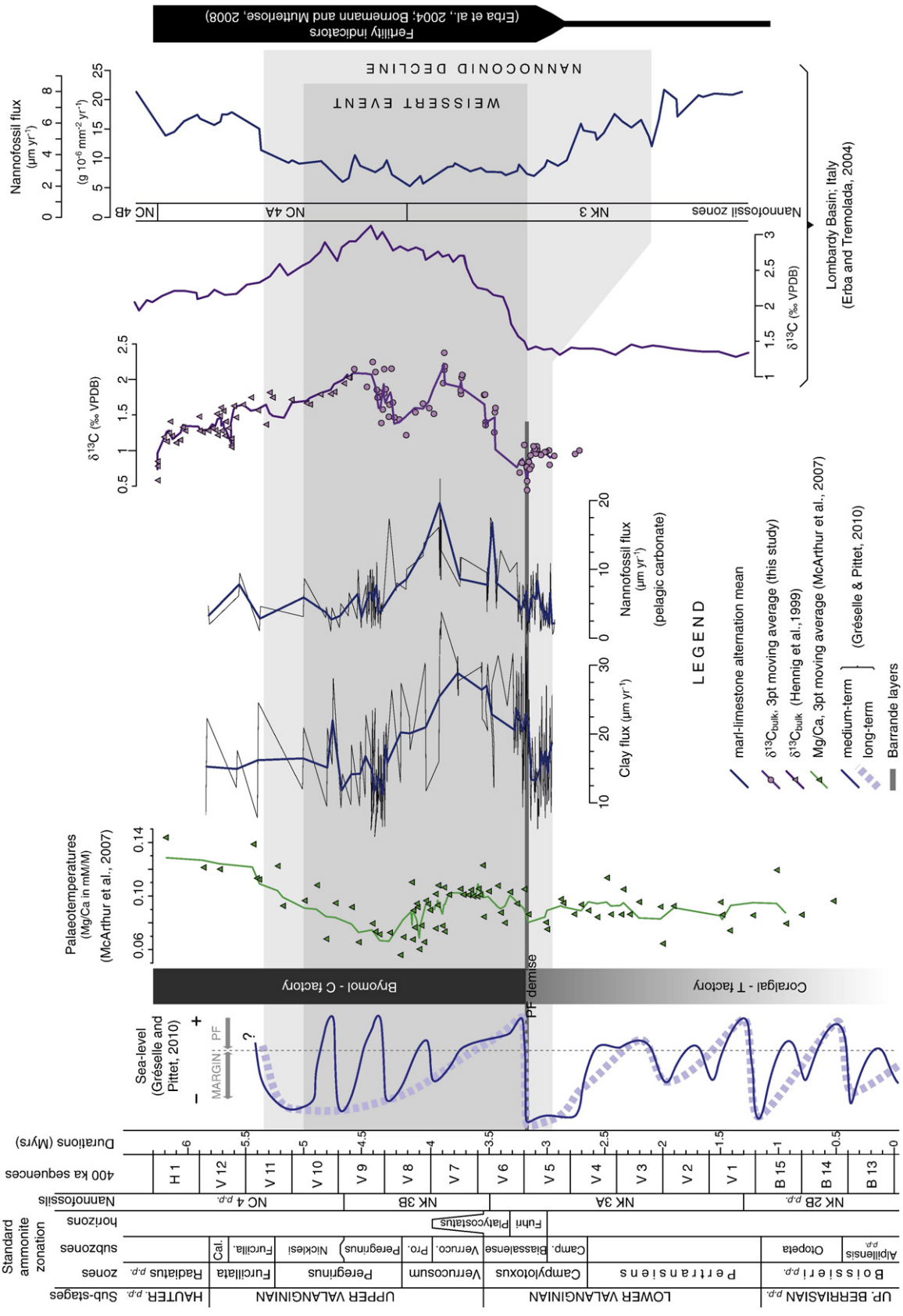

Fig. 8. Evolution of the clay and pelagic carbonate accumulation rates, carbon isotopes, paleotemperatures and sea-level for the Vocontian Basin compared with the evolution of nannofossil flux and carbon isotopes in the Lombardy Basin (Italy; Erba and Tremolada, 2004). Carbon isotope data from the uppermost Peregrinus Subzone to the Hauterivian (*A. radiatus* Zone) from Hennig et al. (1999; triangles). Palaeotemperatures and 3-point moving average (solid line) are data from the Vocontian Basin from McArthur et al. (2007); McArthur et al. (2007) data from Spain were not used in this work. Sections and sample numbers are Vergol (45), La Charce (2), Angles (6), Les Prades (1), Morenas (20), Serre de la Croix (1), and Source de l'Asse de Moriez (5; McArthur et al., 2007). Sea-level fluctuations relative to the Vocontian Basin are from Gréselle and Pittet (2010). See the text for detail. Data from the Vocontian and Lombardy basins are correlated to the ignition and the maximum values of the $\delta^{13}C$ positive excursion.

Svalbard (Price and Nunn, 2010). Moreover, several studies suggest the development of high-latitudinal ice caps during the Late Valanginian (Price, 1999; Gréselle and Pittet, 2010 and references therein). Numeric modeling indicates an increase in climate humidity at low-to-intermediate latitudes (Price et al., 1998). Climate modeling by Chumakov (1995) proposed a more humid and warmer climate for latitudes around 30°N, corresponding to the position of the Vocontian Basin and of surroundings mountain ranges. The regional response of Valanginian glaciations would then have been a more humid climate inducing more intense continental weathering and increase in both clay and nutrient input in the Vocontian Basin. This change would have enhanced carbonate production by nannofossils in the basin whereas shallow-water carbonate production would have been drastically reduced, illustrating the Valanginian carbonate platform crisis. This migration of latitudinal belts probably did not affect southernmore latitudes, where the Lombardy Basin was located. In this area, situated more distally from continental areas, the increase in coccolith fluxes was likely less effective than in the Vocontian Basin, although the general trophic conditions were high during the Weissert Event (Erba and Tremolada, 2004).

6. Conclusions

This study of the Vocontian Basin documents for the first time the specific response of both basin and platform carbonate systems during the Valanginian Weissert Event, and provides new time-controlled sedimentological and palaeoenvironmental information. Calculation of accumulation rates of the pelagic and non-pelagic carbonates, and of clays deposited in basinal settings allows us to better constrain the evolution of both carbonate production in shallow-water and in pelagic realms. Principal outcomes are the following:

(1) Shallow-water platform and deeper-water basin systems reacted differently to the higher nutrient input to the oceans. First, a decline in *Nannoconus* absolute abundance is recorded in the basin, whereas carbonate production on the platform was not particularly affected. Changes in carbonate production on both the platform and the basin occurred 100 kyr later the Nannoconid decline and represent a synchronous response of the two carbonate systems to the same environmental perturbation. The pelagic carbonate production mainly supported by nannofossils, especially coccoliths, increased at the same time as the carbonate production on the platform decreased with oligotrophic producers being replaced by heterozoans.

(2) The first peak of the positive carbon isotope excursion characterizing the Weissert Event is linked to an enhanced primary productivity by calcareous nannofossils in the basin. The pelagic carbonate production by nannofossils was stimulated by an increased influx of nutrients due to intensified continental weathering and run-off.

(3) The second maximum of the carbon isotope excursion marking the end of the Weissert Event is most probably linked to a still high primary productivity. This was likely mainly supported by non-calcifying organisms, as the abundance of nannofossils tends to decrease after its maximum. The second peak of the positive carbon isotope excursion is synchronous with the thermal minimum recorded worldwide.

(4) Both the increase in climate humidity, invoked here to explain intensification of continental weathering observed in the Vocontian Basin, and the cooling event in the Late Valanginian represent a global climate change. The migration of latitudinal climate belt could have been triggered by the development of high-latitude ice caps starting in the Early Valanginian. In a context of global climate changes, the response of nannofossil fluxes was different in basins located at different paleolatitudes due to local paleoceanographic conditions.

Acknowledgments

We are grateful to Raphaël Morard, Vincent Perrier and Ulrich Heimhofer for their kind help in the field. We also thank John McArthur who kindly provided stable isotope and Mg/Ca ratios published in 2007. We would like to thank Karl Föllmi, Finn Surlyk and an anonymous reviewer who helped to improve the quality of the present work. This study was funded by the INSU-CNRS French program “ECLIPSE II”, SYSTER and INTERRVIE.

References

Adatte, T., Stinnesbeck, W., Hubberten, H., Remane, J., Lopez-Oliva, J.G., 2001. Correlation of a Valanginian stable isotopic excursion in northeastern Mexico with the European Tethys. American Association of Petroleum Geologists Memoir 75, 371–388.

Arthur, M.A., Schlanger, S.O., Jenkyns, H.C., 1987. The Cenomanian–Turonian oceanic anoxic event: palaeoceanographic controls on organic matter production and preservation. In: Brooks, J., Fleet, A.J. (Eds.), Marine Petroleum Source Rocks, pp. 401–420.

Bartolini, A., 2003. Cretaceous radiolarian biochronolgy and carbon isotope stratigraphy of ODP Site 1149 (Northwestern Pacific, Nadezhda Basin). Proceedings of the Ocean Drilling Program. Scientific Results 185, 1–17.

Beaufort, L., 1991. Adaptation of the random settling method for quantitative studies of calcareous nannofossils. Micropaleontology 37, 415–418.

Berger, A., Loutre, M.-F., 1994. Astronomical forcing through geological time. International Association of Sedimentologists Special Publications 19, 15–24.

Bersezio, R., Erba, E., Gorza, M., Riva, A., 2002. Berriasian–Aptian black shales of the Maiolica formation (Lombardian Basin, Southern Alps, Northern Italy): local to global events. Palaeogeography, Palaeoclimatology, Palaeoecology 180, 253–275.

Betzler, C., Reijmer, J.J.G., Bernet, K., Eberli, G.P., Anselmetti, F., 1999. Sedimentary patterns and geometries of the Bahamian outer carbonate ramp (Miocene–Lower Pliocene, Great Bahama Bank). Sedimentology 46, 1127–1143.

Blakey, R., 2005. http://jan.ucc.nau.edu/~rcb7/2005.

Bornemann, A., Mutterlose, J., 2008. Calcareous nannofossil and $\delta^{13}C$ records from the Early Cretaceous of the Western Atlantic Ocean: evidence for enhanced fertilization across the Berriasian–Valanginan transition. Palaios 23, 821–832.

Bornemann, A., Aschwer, U., Mutterlose, J., 2003. The impact of calcareous nannofossils on the pelagic carbonate accumulation across the Jurassic–Cretaceous boundary. Palaeogeography, Palaeoclimatology, Palaeoecology 199, 187–228.

Bralower, T.J., Premoli Silva, I., Malone, M.J., 2002. Leg 198. Proceedings of the Ocean Drilling Program: Initial reports, 198, p. 148.

Channell, J.E.T., Erba, E., Lini, A., 1993. Magnetostratigraphic calibration of the Late Valanginian carbon isotope event in pelagic limestones from northern Italy and Switzerland. Earth and Planetary Science Letters 118, 145–166.

Chumakov, N.M., 1995. Climatic zones in the middle of the Cretaceous period. Stratigraphy and Geological Correlations 3, 3–14.

Cotillon, P., Rio, M., 1984. Cyclic sedimentation in the Cretaceous of Deep Sea Drilling Project sites 535 and 540 (Gulf of Mexico), 534 (central Atlantic), and in the Vocontian Basin (France). In: Buffler, R.T., Schlager, W., Bowdler, J.L., Cotillon, P., Halley, R.B., Kinoshita, H., Magoon, L.B.I., McNulty, C.L., Patton, J.W., Premoli Silva, I., Suarez–Otmara, A., Testarmata, M.M., Tyson, R.V., Watkins, D.K., Pisciotto, K.A. (Eds.), Initial Reports of the Deep Sea Drilling Project, Washington, pp. 339–376.

Cotillon, P., Ferry, S., Gaillard, C., Jautée, E., Latreille, G., Rio, M., 1980. Fluctuation des paramètres du milieu marin dans le domaine vocontien (France Sud–est) au Crétacé inférieur: mise en évidence par l'étude des formations marno–calcaires alternantes. Bulletin de la Société Géologique de France 7 t.XXII, 735–744.

Droxler, A.W., Schlager, W., 1985. Glacial versus interglacial sedimentation rates and turbidite frequency in the Bahamas. Geology 13, 799–802.

Duchamp-Alphonse, S., Gardin, S., Fiet, N., Bartolini, A., Blamart, D., Pagel, M., 2007. Fertilization of the northwestern Tethys (Vocontian basin, SE France) during the Valanginian carbon isotope perturbation: evidence from calcareous nannofossils and trace element data. Palaeogeography, Palaeoclimatology, Palaeoecology 243, 132–151.

Eder, W., 1982. Diagenetic redistribution of carbonate, a process in forming limestone–marl alternations (Devonian and Carboniferous, Rheinisches Schiefergebirge, W. Germany). In: Einsele, G., Seilacher, A. (Eds.), Cycles and Even Stratification. Springer, Berlin, pp. 98–112.

Einsele, G., 2000. Sedimentary basins. Evolution, Facies, and Sediment Budget. Springer.

Einsele, G., Ricken, W., 1991. Limestone–marl alternations—an overview. In: Einsele, G., Ricken, W., Seilacher, A. (Eds.), Springer, pp. 377–382.

Elder, W.P., Gustason, E.R., Sageman, B.B., 1994. Correlation of basinal carbonate cycles to nearshore parasequences in the Late Cretaceous Greenhorn Seaway, Western Interior, U.S. Geological Society of America Bulletin 106, 892–902.

Emmanuel, L., Renard, M., 1993. Carbonate geochemistry (Mn, ∂13 C, ∂18O) of the Late Tithonian–Berriasian pelagic limestones of the Vocontian Through (SE France). Bull. Cent. Rech. Explor.–Prod. Elf–Aquitaine, 17/1, pp. 205–221.

Erba, E., Tremolada, F., 2004. Nannofossil carbonate fluxes during the Early Cretaceous: phytoplankton response to nutrification episodes, atmospheric CO2, and anoxia. Paleoceanography 19. doi:10.1029/2003PA000884.

Erba, E., Bartolini, A., Larson, R.L., 2004. Valanginian Weissert oceanic anoxic event. Geology 32, 149–152.

Ferry, S., 1991. Une alternative au modèle de stratigraphie séquentielle d'Exxon: la modulation tectono–climatique des cycles orbitaux. Géologie Alpine H.S. 18, 47–99.

Föllmi, K.B., 1995. 160 m.y. record of marine sedimentary phosphorus burial: coupling of climate and continental weathering under greenhouse and icehouse conditions. Geology 23, 503–506.
Föllmi, K.B., 1996. The Phosphorus cycle, phosphogenesis and marine phosphate-rich deposits. Earth–Science Reviews 40, 55–124.
Föllmi, K.B., Weissert, H., Bisping, M., Funk, H., 1994. Phosphogenesis, carbon–isotope stratigraphy, and carbonate–platform evolution along the Lower Cretaceous northern Tethyan margin. Geological Society of America Bulletin 106, 729–746.
Föllmi, K.B., Godet, A., Bodin, S., Linder, P., 2006. Interactions between environmental change and shallow water carbonate buildup along the northern Tethyan margin and their impact on the Early Cretaceous carbon isotope record. Paleoceanography 21, PA4211. doi:10.1029/2006PA001313.
Funk, H., Föllmi, K.B., Mohr, H., 1993. Evolution of the Tithonian–Aptian carbonate platform along the northern Tethyan margin, eastern helvetic alps. American Association of Petroleum Geologists Memoir 56, 387–407.
Geisen, M., Bollman, J., Herrle, J.O., Mutterlose, J., Young, J.R., 1999. Calibration of the random settling technique for calculation of absolute abundances of calcareous nannoplankton. Micropaleontology 45, 437–442.
Giraud, F., Beaufort, L., Cotillon, P., 1995. Periodicities of carbonate cycles in the Valanginian of the Vocontian Trough: a strong obliquity control. Geological Society Special Publication 85, 143–164.
Gradstein, F.M., Agterberg, F.P., Ogg, J.G., Hardenbol, J., van Veen, P., Thierry, J., Huang, Z., 1994. A mesozoic time scale. Journal of Geophysical Research 99, 24051–24074.
Gradstein, F.M., Ogg, J.G., Smith, A.G., 2004. A Geologic Time Scale 2004. Cambridge University Press.
Gréselle, B., Pittet, B., 2010. Sea-level reconstructions from the Peri–Vocontian Zone (SE France) point to Valanginian glacio–eustasy. Sedimentology 57, 1640–1684.
Gröcke, D.R., Price, G.D., Robinson, S.A., Baraboshkin, E., Mutterlose, J., Ruffell, A.H., 2005. The Upper Valanginian (Early Cretaceous) positive carbon–isotope event recorded in terrestrial plants. Earth and Planetary Science Letters 240, 495–509.
Harris, P.M., Frost, S.H., Seiglie, G.A., Schneidermann, N., 1984. Regional unconformities and depositional cycles, Cretaceous of the Arabian peninsula. American Association of Petroleum Geologists Memoir 36, 67–80.
Hennig, S., Weissert, H., Bulot, L.G., 1999. C–isotope stratigraphy, a calibration tool between ammonite- and magnetostratigraphy: the Valanginian–Hauterivian transition. Geologica Carpathica 50, 91–96.
Hoedemaeker, P.J., Reboulet, S., Aquirre–Urreta, M.B., Alsen, P., Aoutem, M., Atrops, F., Barragan, R., Company, M., Gonzalez Arreola, C., Klein, J., Lukeneder, A., Ploch, I., Raisossadat, N., Rawson, P.F., Ropolo, P., Vasicek, Z., Vermeulen, J., Wippich, M.G.E., 2003. Report on the 1st International Workshop of the IUGS Lower Cretaceous Ammonite Working Group, the 'Kilian Group' (Lyon, 11 July 2002). Cretaceous Research 24, 89–94.
Krobicki, M., Wierzbowski, A., 1996. New data on stratigraphy of the Spisz Limestone Formation (Valanginian) and the brachiopod succession in the lowermost Cretaceous of the Pieniny Klippen Belt, Carpathians, Poland. Studia Geologica Polonica 109, 53–67.
Laurin, J., Ulicny, D., 2004. Controls on a shallow-water hemipelagic carbonate system adjacent to a siliciclastic margin: example from Late Turonian of Central Europe. Journal of Sedimentary Research 74, 697–717.
Lees, J.A., Bown, P.R., Mattioli, E., 2005. Problems with proxies? Cautionary tales of calcareous nannofossil paleoenvironmental indicators. In: Aubry, M.-P. (Ed.), Approach to Paleobiodiversity, Mesozoic Calcareous Nannoplankton. American Museum of natural History, New York, pp. 333–343.
Lini, A., 1994. *Early Cretaceous carbon isotope stratigraphy of the Maiolica Formation, Southern Alps (Northern Italy and Southern Switzerland): stratigraphic and paleoenvironmental significance*, Diss. Naturwiss., ETH Zürich.
Lini, A., Weissert, H., Erba, E., 1992. The Valanginian carbon isotope event: a first episode of greenhouse climate conditions during the Cretaceous. Terra Nova 4, 374–384.
Masse, J.-P., 1993. Valanginian–Early Aptian carbonate platforms from Provence, southeastern France. In: Simo, J.A.T., Scott, R.W., Masse, J.-P. (Eds.), Cretaceous Carbonate Platform, pp. 363–374.
Masse, J.-P., Philip, J.M., 1981. Cretaceous coral–rudistid buildups of France. American Association of Petroleum Geologists Memoir, 56, pp. 363–374.
McArthur, J.M., Janssen, N.M., Reboulet, S., Leng, M.J., Thirlwall, M.F., Van de Schootbrugge, B., 2007. Palaeotemperatures, polar ice-volume, and isotope stratigraphy (Mg/Ca, δ18O, δ13C, 87Sr/86Sr): the Early Cretaceous (Berriasian, Valanginian, Hauterivian). Palaeogeography, Palaeoclimatology, Palaeoecology 248, 391–430.
Munnecke, A., Samtleben, C., 1996. The formation of micritic limestones and the development of limestone–marl alternations in the Silurian of Gotland, Sweden. Facies 34, 159–176.
Munnecke, A., Westphal, H., Elrick, M., Reijmer, J.J.G., 2001. The mineralogical composition of precursor sediments of calcareous rhytmites: a new approach. International Journal of Earth Sciences 90, 795–812.
Mutterlose, J., Bornemann, A., Herrle, J.O., 2005. Mesozoic calcareous nannofossils—state of the art. Paläontologische Zeitschrift 79, 113–133.
Ogg, J.G., Ogg, G., Gradstein, F.M., 2008. The Concise Geological Time Scale. Cambridge University Press, Cambridge9780521898492. ed.
Olivier, N., Pittet, B., Mattioli, E., 2004. Palaeoenvironmental control on sponge–microbialite reefs and contemporaneous deep-shelf marl–limestone deposition (Late Oxfordian, southern Germany). Palaeogeography, Palaeoclimatology, Palaeoecology 212, 233–263.
Peate, D.W., 2009. Global dispersal of Pb by large-volume silicic eruptions in the Parañá–Etendeka large igneous province. Geology 37, 1071–1074.
Pittet, B., Strasser, A., 1998. Long-distance correlations by sequence stratigraphy and cyclostratigraphy: examples and implications (Oxfordian from the Swiss Jura, Spain and Normandy). Geologische Rundschau 86, 852–874.
Podlaha, O.G., Mutterlose, J., Veizer, J., 1998. Preservation of $\delta^{18}O$ and $\delta^{13}C$ in belemnite rostra from the Jurassic/Early Cretaceous successions. American Journal of Science 298, 324–347.
Price, G.D., 1999. The evidence and implications of polar ice during the Mesozoic. Earth–Science Reviews 48, 183–210.
Price, G.D., Mutterlose, J., 2004. Isotopic signals from late Jurassic–early Cretaceous (Volgian–Valanginian) sub–Arctic belemnites, Yatria River, Western Siberia. Journal of the Geological Society of London 161, 959–968.
Price, G.D., Nunn, E.V., 2010. Valanginian isotope variation in glendonites and belemnites from Artic Svalbard: transient glacial temperatures during the Cretaceous greenhouse. Geology 38, 251–254.
Price, G.D., Valdes, P.J., Sellwood, B.W., 1998. A comparison of GCM simulated Cretaceous 'greenhouse' and 'icehouse' climates: implications for the sedimentary record. Palaeogeography, Palaeoclimatology, Palaeoecology 142, 123–138.
Pucéat, E., Lecuyer, C., Sheppard, S.M.F., Dromart, G., Reboulet, S., Grandjean, P., 2003. Thermal evolution of Cretaceous Tethyan marine waters inferred from oxygen isotope composition of fish tooth enamels. Paleoceanography 18, 1029. doi:10.1029/2002PA000823.
Reboulet, S., 1996. L'évolution des ammonites du Valanginien–Hauterivien inférieur du bassin vocontien et de la plate–forme provençale (sud–est de la France) : relations avec la stratigraphie séquentielle et implications biostratigraphiques. Thèse. Documents du Centre des Sciences de la Terre de Lyon, 137.
Reboulet, S., Atrops, F., 1995. Rôle du climat sur les migrations et la composition des peuplements d'ammonites du Valanginien supérieur du bassin vocontien (S–E de la France). Geobios 18, 357–365.
Reboulet, S., Atrops, F., 1999. Comments and proposal about the Valanginian Lower Hauterivian ammonite zonation of south-eastern France. Eclogae Geologicae Helvetiae 92, 183–197.
Reboulet, S., Atrops, F., Ferry, S., Schaaf, A., 1992. Renouvellement des ammonites en fosse vocontienne à la limite Valanginien–Hauterivien. Geobios 25, 469–476.
Reboulet, S., Mattioli, E., Pittet, B., Baudin, F., Olivero, D., Proux, O., 2003. Ammonoid and nannoplankton abundance in Valanginian (early Cretaceous) limestone–marl successions from the southeast France Basin: carbonate dilution or productivity? Palaeogeography, Palaeoclimatology, Palaeoecology 201, 113–139.
Reboulet, S., Hoedemaeker, P.J.r., Aguirre-Ureta, M.B., Alsen, P., Atrops, F., Baraboshkin, E., Company, M., Delanoy, G., Dutour, Y., Klein, J., Latil, J.-L., Lukeneder, A., Mitta, V., Mourgues, F.A., Ploch, I., Raisossadat, N., Ropolo, P., Sandoval, J., Tavera, J.M., Vasicek, Z., Vermeulen, J., 2006. Report on the 2nd international meeting of the IUGS lower Cretaceous ammonite working group, the "Kilian Group" (Neuchâtel, Switzerland, 8 September 2005). Cretaceous Research 27, 712–715.
Reboulet, S., Klein, J., Barragan, R., Company, M., Gonzalez Arreola, C., Lukeneder, A., Raisossadat, N., Sandoval, J., Szives, O., Tavera, J.M., Vasicek, Z., Vermeulen, J., 2009. Report on the 3rd International Meeting of the IUGS Lower Cretaceous Ammonite Working Group, the "Killian Group" (Vienna, Austria, 15th April 2008). Cretaceous Research 30, 496–502.
Reijmer, J.J.G., Schlager, W., Droxler, A.W., 1988. Site 632: Pliocene–Pleistocene sedimentation cycles in a Bahamian basin. Proceedings of the Ocean Drilling Program. Scientific Results 101, 213–220.
Rendle-Bühring, R.H., Reijmer, J.J.G., 2005. Controls on grain-size patterns in periplatform carbonates: marginal setting versus glacio-eustacy. Sedimentary Geology 175, 99–113.
Ricken, W., 1986. Diagenetic bedding: a model for limestone–marl alternations. Lectures Notes in Earth Sciences 6, 210.
Ricken, W., 1994. Complex rhythmic sedimentation related to third-order sea-level variations: Upper Cretaceous, Western Interior Basin, USA. International Association of Sedimentologists Special Publications 19, 167–193.
Roth, P., 1984. Mesozoic pelagic carbonate and organic carbon deposition; causes and effects. Eos, Transactions, AGU, San Francisco, CA, United States, p. 977.
Schlager, W., 1981. The paradox of drowned reefs and carbonate platforms. Geological Society of America Bulletin 92, 197–211.
Schlager, W., 2000. Sedimentation rates and growth potential of tropical, cool-water and mud-mound carbonate factories. In: Insalaco, E., Skelton, P.W., Palmer, T.J. (Eds.), Carbonate Platform Systems: Components and Interactions, pp. 217–227.
Schlager, W., 2003. Benthic carbonate factories of the Phanerozoic. International Journal of Earth Sciences 92, 445–464.
Schlager, W., Reijmer, J.J.G., Droxler, A.W., 1994. Highstand shedding of carbonate platforms. Journal of Sedimentary Research B64, 270–281.
Scholle, P.A., Arthur, M.A., 1980. Carbon isotope fluctuations in Cretaceous pelagic limestones: potential stratigraphic and petroleum exploration tool. American Association of Petroleum Geologists Bulletin 64, 67–87.
Sprovieri, M., Coccioni, R., Lirer, F., Pelosi, N., Lozar, F., 2006. Orbital tuning of a lower Cretaceous composite record (Maiolica Formation, central Italy). Paleoceanography 21, PA 4212. doi:10.1029/2005PA001224.
Stein, R., Rullkötter, J., Welte, D.H., 1986. Accumulation of organic-carbon-rich sediments in the Late Jurassic and Cretaceous Atlantic Ocean—a synthesis. Chemical Geology 56, 1–32.
Stoll, H.M., Schrag, D.P., 2001. Sr/Ca variations in Cretaceous carbonates: relation to productivity and sea level changes. Palaeogeography, Palaeoclimatology, Palaeoecology 168, 311–336.
Strasser, A., Pittet, B., Hillgärtner, H., Pasquier, J.-B., 1999. Depositional sequences in shallow carbonate-dominated sedimentary systems: concepts for a high-resolution analysis. Sedimentary Geology 128, 201–221.
Summerhayes, C.P., Masran, T.C., 1983. Organic facies of Cretaceous and Jurassic sediments from Deep Sea Drilling Project Site 534 in the Blake–Bahama Basin, western North Atlantic. Initial Reports of the Deep Sea Drilling Project 76, 469–480.
Thiede, D.S., Vasconcelos, P.M., 2010. Parañá flood basalts: rapid extrusion hypothesis confirmed by new 40Ar/39Ar results. Geology 38, 747–750.

Tremolada, F., Young, J.R., 2002. Volume calculation of Cretaceous coccoliths and nannoliths. Journal of Nannoplankton Research 24, 199–202.

Van de Schootbrugge, B., Föllmi, K.B., Bulot, L.G., Burns, S.J., 2000. Paleoceanographic changes during the early Cretaceous (Valanginian–Hauterivian): evidences from oxygen and carbon stable isotopes. Earth and Planetary Science Letters 181, 15–31.

Van de Schootbrugge, B., Kuhn, O., Adatte, T., Steinmann, P., Föllmi, K.B., 2003. Decoupling of P- and C_{org}–burial following Early Cretaceous (Valanginian–Hauterivian) platform drowning along the NW Tethyan margin. Palaeogeography, Palaeoclimatology, Palaeoecology 199, 315–331.

Wachter, E.A., Hayes, J.M., 1985. Exchange of oxygen isotopes in carbon dioxide–phosphoric acid systems. Chemical Geology 52, 365–374.

Weissert, H., Erba, E., 2004. Volcanism, CO2 and palaeoclimate: a Late Jurassic–Early Cretaceous carbon and oxygen isotope record. Journal of the Geological Society of London 161, 695–702.

Weissert, H., Lini, A., Föllmi, K.B., Kuhn, O., 1998. Correlation of Early Cretaceous carbon isotope stratigraphy and platform drowning events: a possible link? Palaeogeography, Palaeoclimatology, Palaeoecology 137, 189–203.

Westermann, S., Föllmi, K.B., Adatte, T., Matera, V., Schnyder, J., Fleitmann, D., Fiet, N., Ploch, I., Duchamp-Alphonse, S., 2010. The Valanginian $\delta^{13}C$ excursion may not be an expression of a global oceanic anoxic event. Earth and Planetary Science Letters 290, 118–131.

Williams, J.R., Brawlower, T.J., 1995. Nannofossil assemblages, fine fraction stable isotopes, and the paleocanography of the Valanginian–Barremian (Early Cretaceous) North Sea Basin. Paleoceanography 10, 815–839.

Wilpshaar, M., Leereveld, H., Visscher, H., 1997. Early Cretaceous sedimentary and tectonic development of the Dauphinois Basin (SE France). Cretaceous Research 18, 457–468.

Wortmann, U.G., Weissert, H., 2000. Tying platform drowning to perturbations of the global carbon cycle with a $\delta^{13}C_{org}$–curve from the Valanginian of DSDP Site 416. Terra Nova 12, 289–294.

Zhu, D.-C., Chung, S.-L., Mo, X.-X., Zhao, Z.-D., Niu, Y., Song, B., Yang, Y.-H., 2009. The 132 Ma Comei–Bunbury large igneous province: remnants identified in present-day southeastern Tibet and southwestern Australia. Geology 37, 583–586.